In Vivo Kinetics of Mesenchymal Stem Cells Transplanted into the Knee Joint in a Rat Model Using a Novel Magnetic Method of Localization

Yasunari Ikuta, M.D., Naosuke Kamei, M.D., Ph.D., Masakazu Ishikawa, M.D., Ph.D., Nobuo Adachi, M.D., Ph.D., and Mitsuo Ochi, M.D., Ph.D.

Abstract

We have developed a magnetic system for targeting cells in minimally invasive cell transplantation. Magnetically labeled MSCs (m-MSCs) with nanoscale iron particles can be guided into the desired region by magnetic force from an extracorporeal device. We reported that magnetic targeting of m-MSCs enhances cartilage repair in a mini-pig model. However, the detailed kinetics of these magnetically targeted m-MSCs remain unknown. For clinical use, this aspect should be clarified from a safety standpoint. We therefore investigated the spatial and temporal distribution of the fluorescently-labeled m-MSCs transplanted into the knee joint using *in vivo* fluorescence combined with three-dimensional computed tomographic imaging in a rat model. Although the intraarticularly injected m-MSCs were spread throughout the joint cavity in the absence of magnetic force, the magnetic force caused the injected m-MSCs to accumulate around the chondral lesion. Further examinations including *ex vivo* imaging, histological assessments and reverse transcription polymerase chain reaction revealed that transplanted MSCs were not present in any major organs after intraarticular administration, regardless of magnetic targeting. Our data suggest that m-MSCs can be accumulated efficiently into a chondral lesion using our magnetic targeting system, while none of the intraarticularly transplanted MSCs migrate to other major organs. Clin Trans Sci 2015; Volume 8: 467–474

Keywords: stem cell transplantation, marrow/stem cell transplantation, surgery

Introduction

Mesenchymal stem cells (MSCs) are considered one of the most feasible cell sources for clinical application in regenerative stem cell therapy.[1–4] Previously, Wakitani et al. reported the results of a clinical trial of MSC transplantation for the treatment of human cartilage defects of the knee joint in open surgery.[5] As a minimally invasive approach, some previous reports demonstrated the effectiveness of intraarticular injection of MSCs for the treatment of articular cartilage defects.[6,7] However, only a small proportion of the transplanted MSCs appear likely to contribute to cartilage repair using this treatment approach. In addition, another previous study demonstrated that intraarticular injection of a large number of MSCs caused complications such as formation of loose bodies in a rat model.[8] For safe treatment, appropriate numbers of MSCs must be transplanted efficiently into the joint. We therefore established our original cell delivery system using magnetic force called "magnetic targeting." In this system, MSCs (m-MSCs) magnetically labeled with nanoscale iron particles (ferucarbotran) can be controlled and accumulated in the desired region by the use of magnetic force. Our previous study demonstrated that an external magnetic force was able to deliver m-MSCs to a target region in a rabbit model and a fresh-frozen porcine model.[9] We also reported that m-MSCs were delivered onto degenerative human cartilage by external magnetic force and formed a cell layer in combination with extracellular matrix *in vitro*.[10] As a preclinical study, we studied the repair process of a chronic full-thickness cartilage defect using magnetic targeting of m-MSCs in a miniature swine model. In this study, the magnetic targeting of m-MSCs promoted the repair of the cartilage defect with hyaline-like cartilage.[11] Several previous studies have investigated the distribution of MSCs after intravenous administration. The majority of intravenously injected MSCs become trapped in the lungs at the time of first-pass.[12–16] However, detailed kinetics of intraarticularly injected MSCs with or without magnetic targeting are still not fully understood. Before clinical application, this aspect should be clarified from a safety standpoint. In this study, we therefore aimed to investigate the spatial and temporal distribution of transplanted m-MSCs into the knee joint using *in vivo* fluorescence imaging combined with three-dimensional computed tomographic imaging (3D-CT) in a rat model.

Materials and Methods

The protocol for this study was approved by the Ethics Committee for Experimental Animals of Hiroshima University. All animal experiments were carried out under the guidelines stipulated by the Institutional Animal Care and Use Committee.

Cell culture

Human MSCs frozen at passage 2 were purchased (Lonza Japan Ltd, Tokyo, Japan) and cultured at 37°C with 5% CO_2 in MSC growth medium (MSCGM BulletKit; Lonza). The MSCs were passaged and split before reaching confluence, and fourth passage human MSCs were used for all experiments.

Cell labeling (magnetic and fluorescent labeling)

Dulbecco's modified eagle medium (DMEM), 15% fetal bovine serum (FBS) and 1% antibiotic-antimycotic mixed stock solution (Nacalai Tesque, Inc., Kyoto, Japan) were equilibrated at 37°C and 5% CO_2 for at least 30 minutes. Nanoscale iron particles (ferucarbotran; 27.9 mg Fe/mL) (Fujifilm RI Pharma Co., Ltd., Tokyo, Japan) were used for magnetic labeling of the MSCs. Ferucarbotran (35.2 μL) was added to 10 mL of the equilibrated

medium, and the solution was mixed manually for 3 minutes. After mixing, all of the solution was added to the MSCs in the culture dish, and incubated overnight to obtain magnetically labeled cells. XenoLight DiR (Perkin Elmer, Inc., Boston, MA, USA) was used for fluorescent labeling of the m-MSCs. XenoLight DiR is a lipophilic near-infrared fluorescent cyanine dye (1,1'-dioctadecyltetramethyl indotricarbocyanine iodide), with absorption and emission peaks at wavelengths of 748 and 780 nm. The magnetically labeled MSCs (m-MSCs) were washed three times with Dulbecco's phosphate buffered saline (DPBS) and trypsinized. DiR was dissolved in ethanol, and this solution was mixed with PBS. The m-MSCs were incubated with 320 μg/mL DiR solution in a 37°C incubator for 30 minutes. After incubation, the m-MSCs were centrifuged and washed with PBS to remove free dye in accordance with the manufacturer's instructions.

Magnetic device

To generate a magnetic field in an objective space, we used a miniature superconducting bulk magnet system (Hitachi Ltd, Ibaraki, Japan). This system produces a magnetic flux density of 3.15 Tesla on the center portion of the vacuum chamber surface, and its magnetic field decreases with increasing distance from the surface. A magnetic flux density of approximately 1.5 Tesla at a distance of 4 mm from the surface of the vacuum chambers was used in this study.

Animals and surgical procedure

Female nude rats (*F344/NJcl-rnu/rnu*) were obtained from CLEA Japan, Inc. (Tokyo, Japan). The rats were randomly divided into two groups of an intravenous administration group (IV; $n = 3$) and an intraarticular administration group ($n = 18$). Furthermore, the intraarticular administration group was subdivided into a normal cartilage subgroup (NC, $n = 6$), a cartilage defect subgroup (CD, $n = 6$), and a magnet subgroup (M, $n = 6$). Intact rats that did not receive cell transplantation were used as the negative control group for histological examination and reverse transcription polymerase chain reaction. The rats were anesthetized using ketamine (100 mg/kg) and xylazine (12 mg/kg) by intraperitoneal administration, and buprenorphine (0.1 mg/kg) by subcutaneous injection. In the intravenous administration group, m-MSCs (5.0×10^5 cells) in 200-μL phosphate-buffered saline (PBS) were injected into the caudal vein. In the intraarticular administration group, surgery was performed at 9 weeks of age with a mean body weight of 151 g (141.2–163.7). After making a straight skin incision in the right knee, the femoral groove was exposed through a medial approach. In the cartilage defect subgroup and the magnet subgroup, a full-thickness articular cartilage defect 2 mm in diameter was created at the femoral groove using a power drill. The knee joint was irrigated with saline solution, and the capsule was tightly sutured using 5–0 nylon. In the normal cartilage subgroup, the capsule was closed without creating a cartilage defect. The m-MSCs (5.0×10^4 cells) in 50 μL PBS were injected into the knee joint using a 29-gauge needle immediately after suturing the capsule. In the normal cartilage subgroup and cartilage defect subgroup, m-MSCs were administered without any magnetic control. In the magnet group, cell transplantation was performed under an external magnetic force (1.5 Tesla), and the center of the magnetic device was applied to the popliteal region for 10 minutes to accumulate the m-MSCs to the cartilage defect.

Fluorescence imaging analysis

Fluorescence imaging was performed using an IVIS spectrum CT (Perkin Elmer, Inc). Living Image 4.3.1 software was used to analyze the images. The filters were configured at 710 nm for excitation and 760 nm for emission. Various cell numbers of fluorescent labeled MSCs (5.0×10^2 to 1.0×10^5) were placed in a 96-well culture dish using serial dilution. An *in vitro* fluorescence assay was performed to evaluate the detection limit of the IVIS spectrum CT system.

Rats were anesthetized before imaging using ketamine and xylazine by intraperitoneal administration except for the initial time. *In vivo* fluorescence imaging was performed at fixed intervals and *ex vivo* imaging was done at 72 hours after surgery for the intravenous administration group. *In vivo* fluorescence images and computed tomography images were acquired without sacrifice immediately and 1, 3, 7, 14, 21, and 28 days after cell transplantation to the knee for the intraarticular administration group. Fluorescence imaging tomography (FLIT) analysis which generates a 3D reconstruction of the distribution of the fluorescent sources was performed to assess the localization of transplanted MSCs.

Rats were sacrificed after *in vivo* imaging at day 28, and major organs: the brain, heart, lungs, liver, spleen, kidneys and the lower limb were removed. *Ex vivo* fluorescence imaging of the major organs was also carried out immediately after sacrifice. Fluorescent signal intensity was measured in the right knee area of each *in vivo* image by delineating the region of interest (ROI) around the cartilage defect area using 3D ROI. The 3D ROI was set using the same scale in all samples, and at a fixed inclination and rotation with reference to the transepicondylar axis, posterior condylar line and anterior cortical line. The center of the 3D ROI was located on the articular cartilage defect of the patellar groove.

Histopathology

The extracted major organs were fixed in 4% paraformaldehyde (Wako Pure Chemical Industries Ltd, Osaka, Japan) at 4°C for 24 hours. The tissues were then placed into 20% sucrose solution overnight. Frozen sections were prepared using Optimal Cutting Temperature (OCT) compound (Sakura Finetek Japan Co., Ltd., Tokyo, Japan). Sections of the major organs were stained with berlin blue using the conventional procedure, and nuclei were stained with nuclear fast red solution (Sigma-Aldrich Japan, Tokyo, Japan). Adjacent sections were stained for human cells by immunofluorescence staining to detect the transplanted human MSCs. Sections were blocked with protein block, serum-free (Dako Japan Inc., Tokyo, Japan) for an hour. An antibody against human-specific mitochondria (EMD Millipore) was used as the primary antibody, diluted in background-reducing antibody diluent (Dako Japan). After washing twice in PBS, sections were stained with primary antibody (1:100) at 4°C overnight. Sections were then washed three times for 5 minutes each time, and incubated with the secondary antibody (1:400); Alexa Fluor 568 goat antimouse IgG antibody (Life Technologies, Frederick, MD, USA) at 4°C overnight. Sections were again washed three times for 5 minutes each before counterstaining with 4,6,-diamidino-2-phenylindole (DAPI) solution for 5 minutes. After washing in PBS, coverslips were applied to the slides using fluoromount/plus (Cosmo Bio Co., Ltd., Tokyo, Japan).
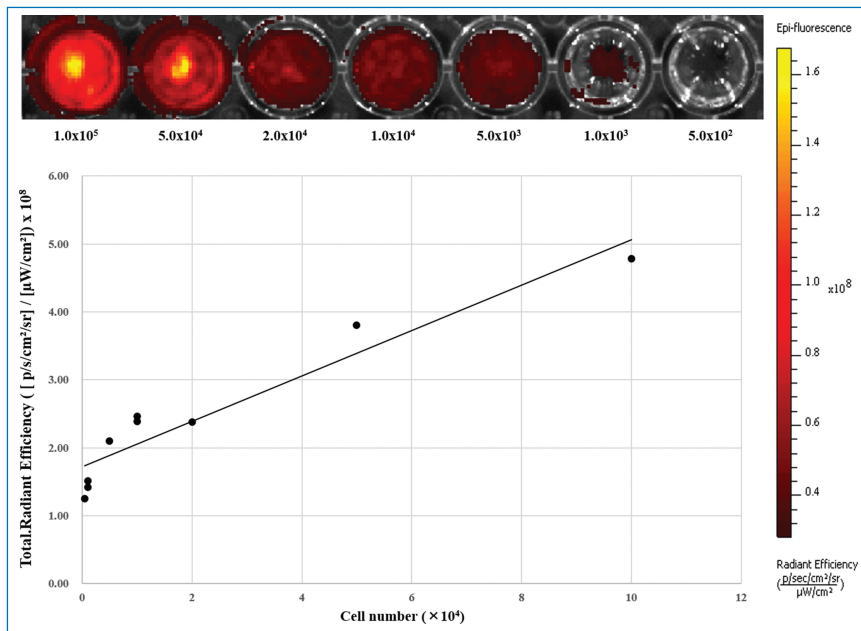
Figure 1. *In vitro* assay of fluorescent intensity in various numbers of fluorescent labeled m-MSCs. The fluorescent intensity is directly proportional to the number of MSCs. No fluorescent signal can be detected with 5.0×10^2 MSCs.
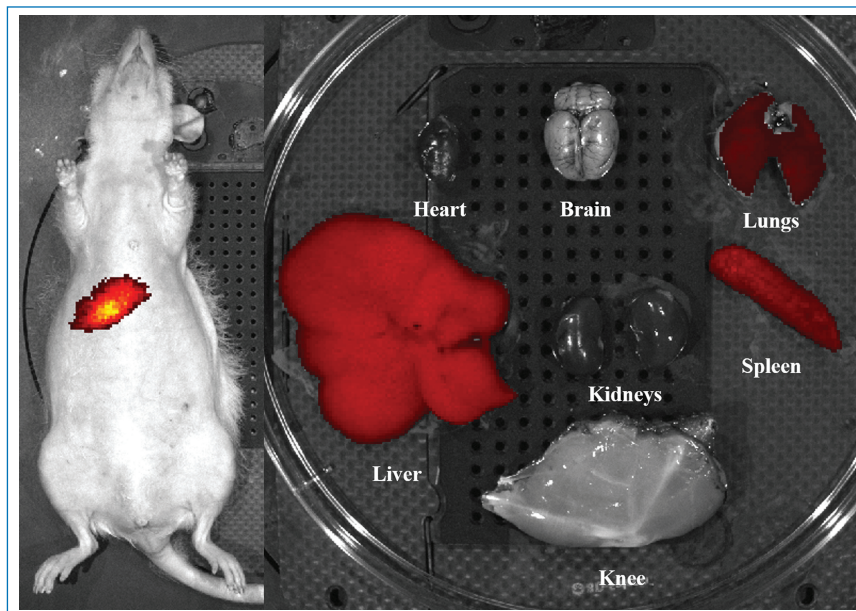

Figure 2. *In vivo* and *ex vivo* imaging of the intravenous administration model at 72 hours after cell transplantation. The fluorescent signal is observed around the border area between the breast and the abdomen in *in vivo* imaging. *Ex vivo* imaging shows pronounced fluorescent signals in the lungs, liver, and spleen.

Reverse transcription-polymerase chain reaction

Reverse transcription-polymerase chain reaction (RT-PCR) was performed to analyze expression of human genes. The removed major organs; brain, heart, lungs, liver, spleen, kidneys, and synovium, were processed using RNA later (Life Technologies), and total RNA was extracted from the tissues using TRIzol (Life Technologies). Complementary DNA was obtained by reverse transcription of equal amounts of RNA per sample (200 ng) using SuperScript VILO Master Mix (Life Technologies) according to the manufacturer's protocol. PCR was performed in a total volume of 10-μL reaction mix and contained 0.025 U/μL Biotaq DNA polymerase (Bioline, London, United Kingdom), 10× NH_4 reaction buffer, 0.8 mM dNTP mix, 2.5 mM $MgCl_2$, 0.2 μM of each primer, and 0.5 μL of cDNA using a PCR thermocycler (GeneAmp PCR system 9700, Life Technologies). Matsumoto et al. previously reported the human-specific primers, and confirmed that there was no interspecies cross-reactivity between human and rat genes.[17] Glyceraldehyde 3-phosphate dehydrogenase (GAPDH) was used to detect the human-specific genes. Primer sequences were as follows: Human GAPDH (596 bp) sense 5-CTGATGCCCCCATGTTCGTC-3, antisense 5-CACCCTGTTGCTGTAG CCAAATTCG-3; rat GAPDH (320 bp) sense 5-GTGCCAGCCTCGTCTCATAGA-3, antisense 5-CGCCAGTAGACTCCACGA CAT-3. The amplification conditions were: initial denaturation at 94°C for 1 minute, and then 35 cycles of 94°C for 30 seconds, 56°C for 1 minute, 72°C for 30 seconds. A final extension step at 72°C for 7 minutes was added after cycling. Five microliters of each PCR product was electrophoresed at 50 V for 30 minutes in 1.5% agarose gel with 1× Tris-borate EDTA buffer, and visualized by an AE-6931GXCL Printgraph (ATTO CORPORATION, Tokyo, Japan).

Statistical analysis

All data are presented as mean and standard deviation (SD). The fluorescent signal intensity of the knee in each intraarticular transplantation group was compared by one-way analysis of variance (ANOVA) with the Tukey–Kramer method for *post hoc* comparison. The p values less than 0.05 were considered significant. Statcel3 software (OMS, Tokyo, Japan) was used for analyses.

Results

In vitro fluorescence assay

The fluorescence intensity of the labeled MSCs changed in proportion to the cell number (*Figure 1*). Small numbers of labeled MSCs less than 1.0×10^3 did not produce a detectable fluorescent signal.

In vivo and *ex vivo* fluorescence imaging

Intravenous administration group

Fluorescently labeled MSCs were administered intravenously as a positive control for migration of transplanted MSCs to major
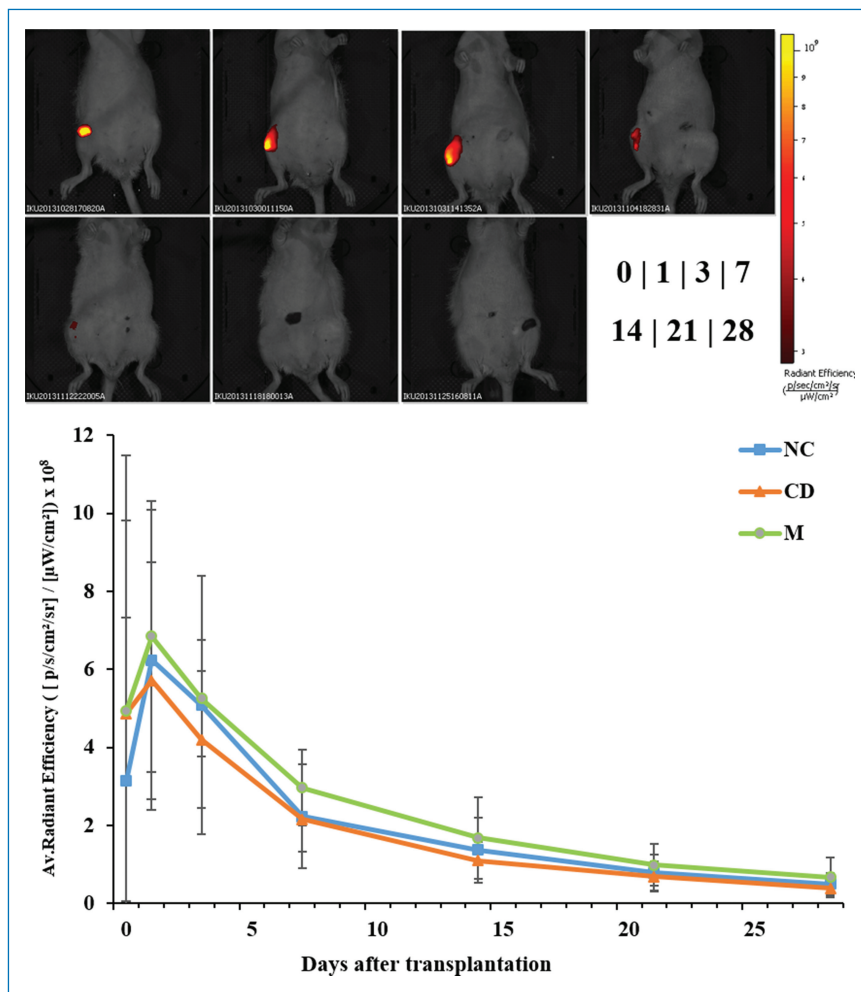
Figure 3. Representative time-dependent changes in fluorescent signals in the normal cartilage subgroup. The graph shows the sequential quantification of fluorescent intensity of the whole knee for each subgroup. The error bars denote the standard deviation of the mean. There is no significant difference in signal intensity among the three subgroups. NC = normal cartilage subgroup; CD = cartilage defect group without magnetic targeting; M = cartilage defect group with magnetic targeting.

accumulated around the chondral lesion site in the magnet subgroup (M) (*Figure 4*). The fluorescent intensity around the femoral groove was also measured by FLIT using 3D ROI. The fluorescent intensity was significantly stronger in the magnet group at day 3 (p = 0.038) and day 7 (p = 0.049) (*Figure 4*). *Ex vivo* imaging did not reveal any fluorescent signals in the extracted major organs including the brain, heart, lungs, liver, spleen, or kidneys, except for the right knee in all subgroups (*Figure 5*).

Histological evaluation

Berlin blue staining
In order to detect the distribution of iron particles derived from transplanted MSCs, tissue sections of the major organs were stained with berlin blue (*Figure 6*). Because the spleen contains endogenous iron, the spleen sections were positively stained by berlin blue in all groups, including the intact model. Apart from the spleen, some positive staining for berlin blue was observed in the lung, liver, and kidneys in the intravenous administration group. In contrast, no berlin blue dye was observed in the intraarticular administration group. Berlin blue staining revealed the absence of iron oxide derived from intraarticularly transplanted MSCs in the major organs (*Figure 6*).

Immunofluorescence staining
To assess the distribution of transplanted human MSCs in the major organs, tissue sections of all the major organs were immunostained with an antibody against human-specific mitochondrial antibodies (*Figure 7*). In the intravenous administration group, many human-specific-mitochondria positive cells were observed in the lungs, and a small number of these cells were also present in the kidney, spleen, and liver. No human-derived cells were present in the major organs of the intraarticular administration group.

RT-PCR
To detect the small number of human MSCs that are undetectable by fluorescent imaging, RT-PCR was performed using human and rat specific GAPDH primers (*Figure 8*). RNA from human MSCs was used as the positive control in all groups. Tissue samples of an intact rat, including brain, heart, lungs, liver, spleen, kidneys, and synovium were used as the negative controls. In addition, the corresponding tissue samples containing 500 human MSCs were used as positive controls. Rat GAPDH was definitely detected in all samples other than human MSCs. In all tissue types, no human GAPDH expression could be detected except in the human MSCs in the negative control group, but were present in all organs of the positive control group. Although the band of human GAPDH could be detected in all tissues in the intravenous administration group, it was never observed in any tissue in any subgroup of the
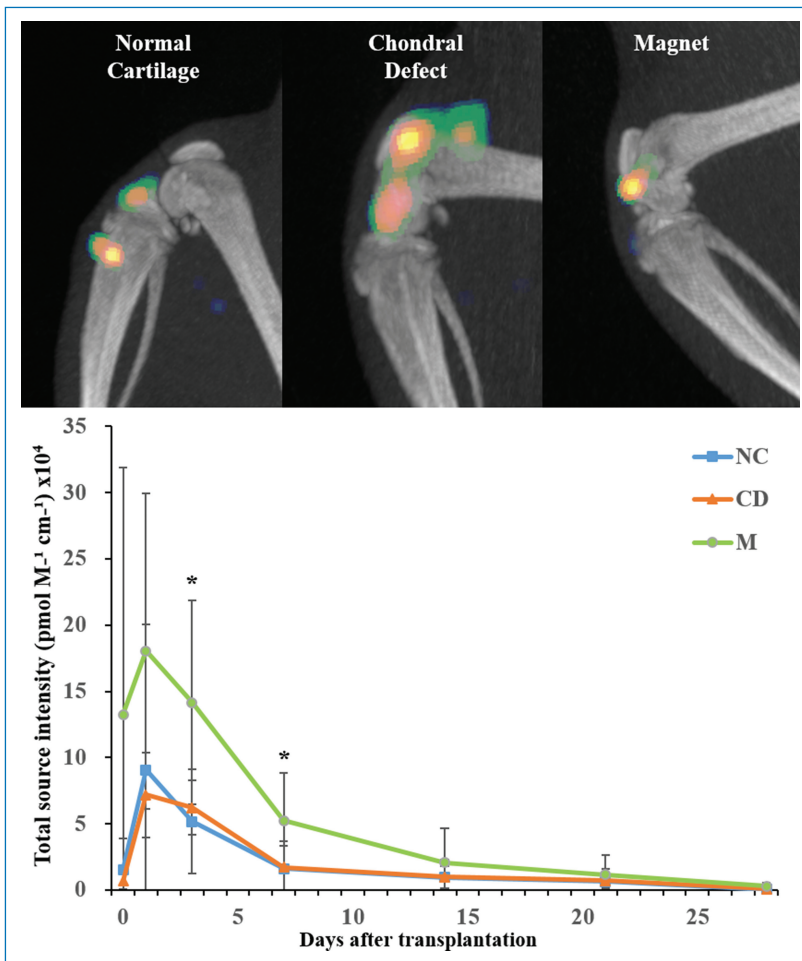
organs. Although the fluorescent signals were not observed immediately after injection, they were detected in the upper abdomen 30 minutes later. The fluorescent intensity gradually increased up to 48 hours after injection, and afterwards decreased. *Ex vivo* imaging revealed that the fluorescent signals were detected only in the lung, liver, and spleen (*Figure 2*).

Intraarticular administration group
The fluorescent signals were detected only around the right knee, and were not detectable in other parts of the body immediately after injection in the intraarticular administration group. The fluorescent intensity peaked at 1 day after injection, and gradually decreased from the 3rd day in all subgroups (*Figure 3*). In contrast, there was no detectable fluorescent signal in the rats injected with the negative control cells without fluorescent labeling (data not shown). There were no significant differences in fluorescent intensity of the whole right knee joint at any time-point among the three subgroups (*Figure 3*). Fluorescence imaging combined with 3D-CT of the right knees showed that the fluorescent signals were diffused in the knee joint in the normal cartilage subgroup (NC) and chondral defect subgroup (CD), but were

Figure 4. Representative images of fluorescence imaging tomography (FLIT) for each subgroup immediately after cell transplantation. The graph shows the sequential quantification of fluorescent intensity around the femoral groove for the each group. Statistical analysis reveals a significant difference at three days (p = 0.038) and seven days (p = 0.049) after cell transplantation. The error bars denote the standard deviation of the mean.
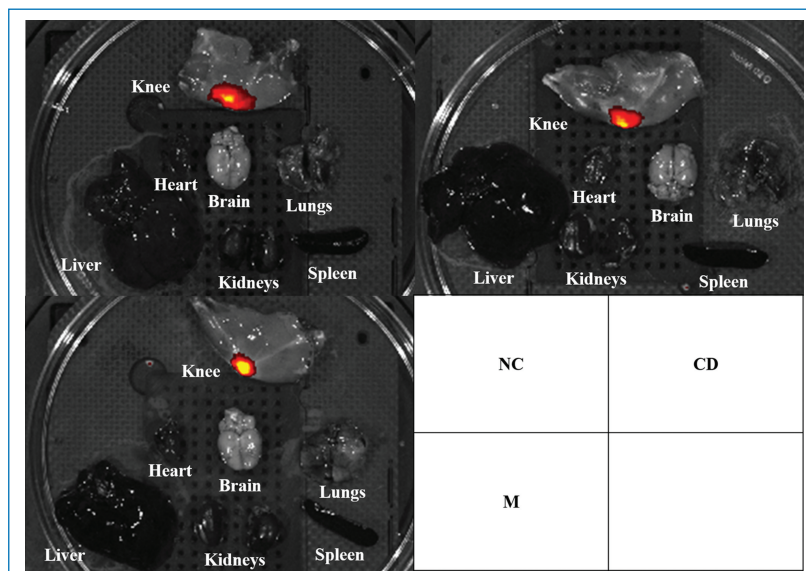

Figure 5. *Ex vivo* imaging of major organs at 28 days following cell transplantation (intraarticular administration model). No fluorescent signals can be obsereved in any major organs except the knee.

intraarticular administration group. These results suggest that intraarticularly transplanted human MSCs did not translocate to the major organs.

Discussion

This study demonstrates two novel findings concerning the kinetics of MSCs transplanted into the knee. First, *in vivo* fluorescent imaging combined with 3D-CT evaluation reveals that the transplanted m-MSCs accumulate around the articular cartilage defect under the influence of the external magnetic targeting system. Second, our data of *in vivo* fluorescent imaging, histological assessments and RT-PCR suggest that none of the intraarticularly injected MSCs or iron particles migrate to the major organs regardless of the presence of an articular cartilage defect or magnetic targeting.

Assessment of *in vivo* fluorescence imaging shows that the existence of an articular cartilage defect or magnetic targeting does not affect the fluorescent signal intensity of the whole knee. As the rat knee is small, conventional *in vivo* imaging cannot show the detailed localization of fluorescent signal in the knee. In contrast, *in vivo* fluorescence imaging combined with 3D-CT shows the presence of diffuse fluorescent signals in the subgroups without magnetic targeting, and accumulation of fluorescent signals around the chondral lesion in the group treated with magnetic targeting. In addition, fluorescent intensity around the femoral groove was strongest in the group treated by intraarticular injection with magnetic targeting up to 7 days after injection. These findings suggest that our magnetic targeting system not only accumulates the intraarticularly injected MSCs but also causes the majority of them to remain around the chondral lesion.

From the point of view of safety, the greatest cause for concern associated with transplantation of m-MSCs is the transfer of injected MSCs and iron particles to the major organs. Migration of a large number of MSCs might induce infarction of major organs, and iron overload might cause organ damage especially in the liver and heart due to free radical production.[18] In this study, *in vivo* fluorescence imaging showed the absence of fluorescent signals in any area of the body except for the right knee joint at several time points up to 28 days after intraarticular injection of fluorescent labeled MSCs. Additionally, *ex vivo* fluorescence imaging, histological assessments and RT-PCR revealed that no transplanted human MSCs or iron particles were present in the major organs at 28 days after intraarticular injection. *In vivo* fluorescence imaging is useful in that it can be constantly assessed in living animals. However, it has limited detection sensitivity. The results of our assessment of the sensitivity of fluorescence imaging suggest that it cannot detect fewer than 1,000 MSCs. Therefore, histological evaluation and
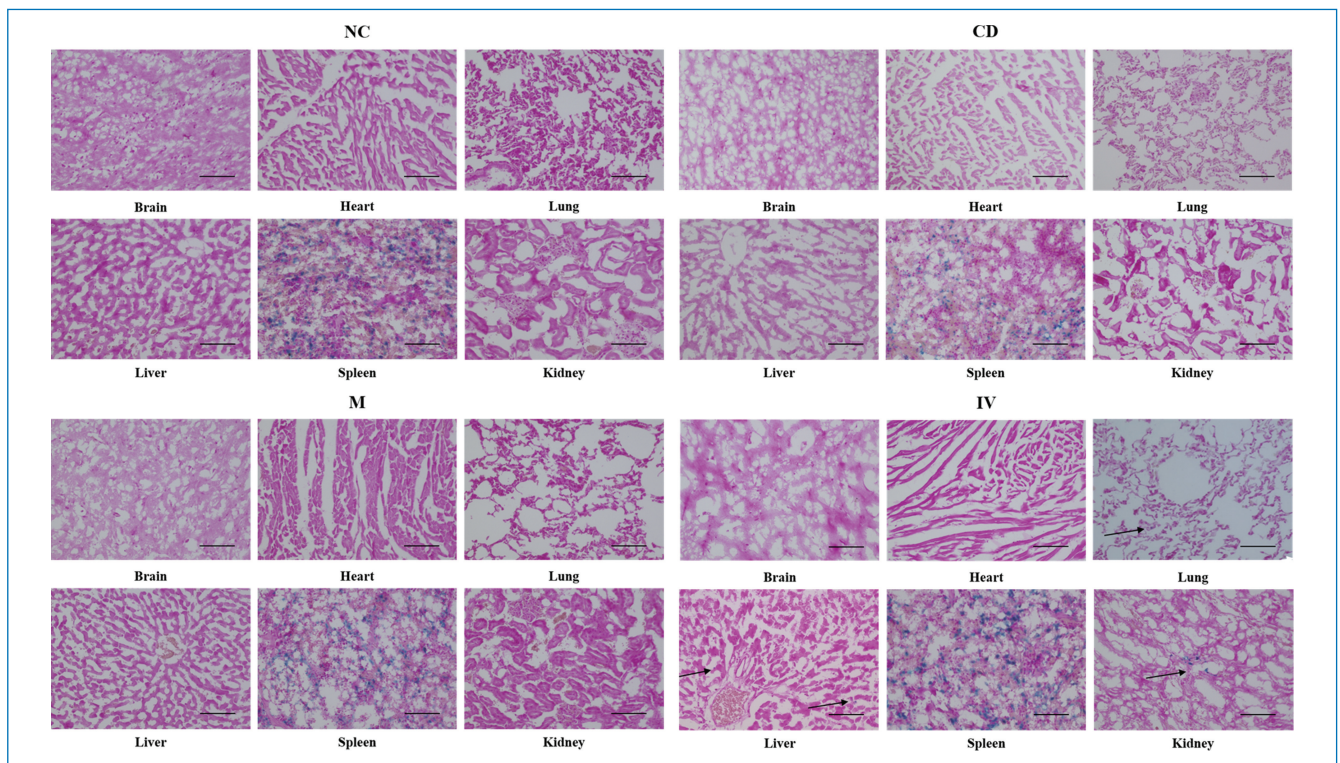
Figure 6. Berlin blue staining at 28 days following cell transplantation in the intraarticular administration model. Berlin blue dye was observed in the spleen sections in all groups. Although a few small patches of berlin blue dye could be seen in the sections of lung, liver, and kidneys in the intravenous administration group, no berlin blue dye was ever observed in any organs except the spleen in all subgroups treated by intraarticular administration. Scale bars: 100 μm.
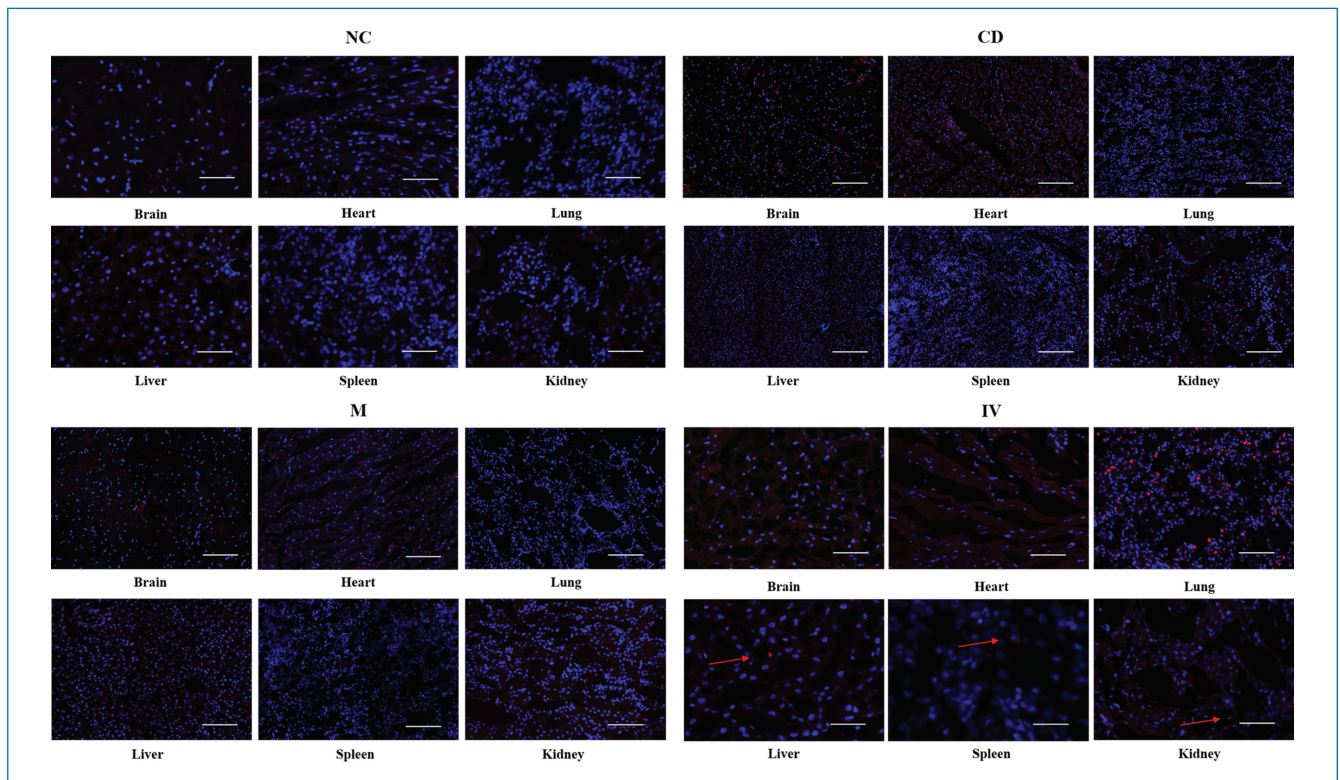

Figure 7. Immunofluorescent staining with antibodies against human-specific mitochondria in the major organs of the intravenous administration model and the intraarticular administration model. Although human-mitochondria-positive cells (red fluorescence and red arrows) can be observed in the lung, liver, spleen, and kidney in the intravenous administration model, these cells cannot be identifed in any organs in any subgroups of the intraarticular administration model. Scale bars: 100 μm.
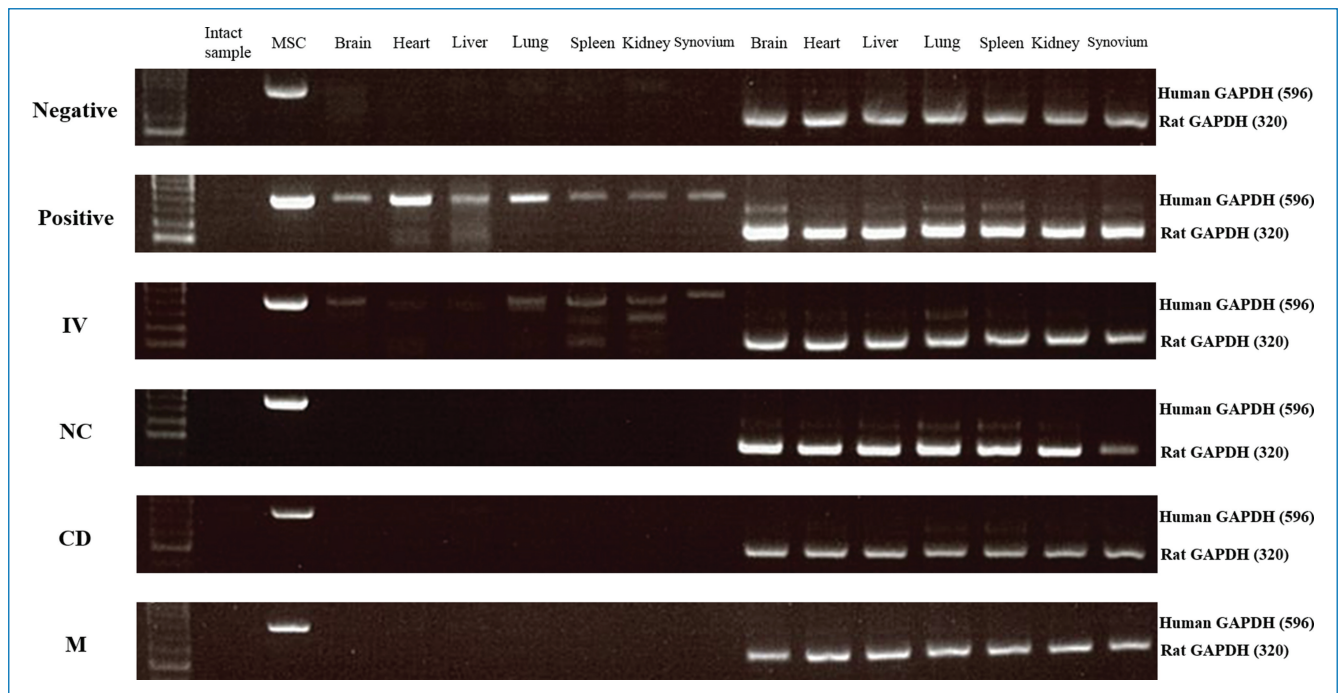
Figure 8. Agarose gel electrophoresis of RT-PCR products. The band of rat GAPDH is definitely observed in all samples except human MSCs. Human GAPDH expression cannot be detected in any samples except for the MSCs, but is present in all the organs in positive control. Although human GAPDH expression could be detected in all organs in the intravenous administration group, it could not be observed in any organs in any subgroup of the intraarticular administration group. Negative: samples of intact model. Positive: five hundred MSCs added to the samples of the intact model.

RT-PCR were performed using tissue samples of major organs in order to detect small numbers of human MSCs. These data in this study strongly support the hypothesis that magnetic targeting of MSCs is a safe treatment.

The management of articular cartilage defects is one of the most challenging clinical problems. The goal of surgical repair is to achieve the regeneration of hyaline cartilage.[19,20] A variety of techniques have been used to treat cartilage defects such as bone marrow stimulation, osteochondral graft and autologous chondrocyte implantation. MSC-based therapies for the regeneration of cartilage have gained popularity over the last few years.[7] Transplantation or injection of MSCs into cartilage defects has been attempted in preclinical and clinical studies.[21] No intraarticular complications were observed during follow-up, and MSCs have safely been applied in a number of clinical trials in humans.[22] MSCs are a promising source of stem cells for tissue repair and gene therapy because of their relative ease of expansion in culture, and their immunologic characteristics.[23] MSCs can differentiate into several different cell types *in vitro*, and act through paracrine mechanisms that might play a role in stimulation of the regenerative process.[24] However, low cell survival and engraftment rate have been the main limiting factors of stem cell-based therapies,[25] and improvement of cell delivery methods is necessary to maximize the regenerative potential of MSCs.[26] To address this issue, we developed an original magnetic cell delivery system to expeditiously localize cells to the target site, and have previously demonstrated that m-MSCs delivered using this system regenerated articular cartilage, bone, muscle, and spinal cord.[9,11,27–30] Kamei et al. showed that m-MSCs delivered using our system promote early regeneration of the cartilage layer and regenerate cartilage in a porcine full thickness cartilage defect model with hyaline-like cartilage.[11] Efficacy of m-MSCs combined with a magnetic cell delivery system for articular cartilage defect repair were thus confirmed in an animal model. This procedure is progressing to the preliminary stages of clinical use. For the realization of clinical use, it is important to confirm the safety of intraarticular transplanted m-MSCs. The *in vivo* kinetics of systemically administered MSCs have already been reported in various studies. Intravenously injected MSCs were mainly trapped in the lungs.[31,32] The homing of MSCs to injured areas was impeded by cell entrapment in the lungs in a myocardial infarction model.[33] MSCs that were injected into the left ventricle evaded trapping in the capillary beds of the lung, and instead were dispersed to the heart, lungs, and kidney glomeruli.[14] The highest levels of engraftment were observed in the pancreas and kidney in a diabetic model.[34] Conversely, *in vivo* kinetics of intraarticularly transplanted MSCs have remained unclear. Therefore, our findings in the present study are helpful in demonstrating that clinical treatment for articular cartilage defects using MSC transplantation with magnetic targeting can be performed safely.

Conclusion
This study showed that the transplanted m-MSCs accumulate around the articular cartilage defect under the influence of the external magnetic targeting system, and none of the intraarticularly injected MSCs or iron particles migrate to the major organs. The findings in this study support that the clinical application of our novel cell targeting system using m-MSCs and a magnetic device can be performed effectively and safely.

References

1. Chen SL, Fang WW, Ye F, Liu YH, Qian J, Shan SJ, Zhang JJ, Chunhua RZ, Liao LM, Lin S, et al. Effect on left ventricular function of intracoronary transplantation of autologous bone marrow mesenchymal stem cell in patients with acute myocardial infarction. *Am J Cardiol*. 2004; 94(1): 92–95.

2. Behfar A, Terzic A. Mesenchymal stem cells: engineering regeneration. *Clin Transl Sci*. 2008; 1(1): 34–35.

3. Sherman LS, Munoz J, Patel SA, Dave MA, Paige I, Rameshwar P. Moving from the laboratory bench to patients' bedside: considerations for effective therapy with stem cells. *Clin Transl Sci*. 2011; 4(5): 380–386.

4. Taghavi S, Sharp TE, 3rd, Duran JM, Makarewich CA, Berretta RM, Starosta T, Kubo H, Barbe M, Houser SR. Autologous c-Kit+ mesenchymal stem cell injections provide superior therapeutic benefit as compared to c-Kit +cardiac-derived stem cells in a feline model of isoproterenol-induced cardiomyopathy. *Clin Transl Sci*. 2015 Feb 11. [Epub ahead of print].

5. Wakitani S, Imoto K, Yamamoto T, Saito M, Murata N, Yoneda M. Human autologous culture expanded bone marrow mesenchymal cell transplantation for repair of cartilage defects in osteoarthritic knees. *Osteoarthritis Cartilage*. 2002; 10(3): 199–206.

6. Nishimori M, Kanaya A, Exham H, Adachi N, Ochi M. Repair of chronic osteochondral defects in the rat. *J Bone Joint Surg Br*. 2006; 88(9): 1236–1244.

7. Lee KB, Hui JH, Song IC, Ardany L, Lee EH. Injectable mesenchymal stem cell therapy for large cartilage defects—a porcine model. *Stem Cells*. 2007; 25(11): 2964–2971.

8. Agung M, Ochi M, Yanada S, Adachi N, Izuta Y, Yamasaki T, Toda K. Mobilization of bone marrow-derived mesenchymal stem cells into the injured tissues after intraarticular injection and their contribution to tissue regeneration. *Knee Surg Sports Traumatol Arthrosc*. 2006; 14(12): 1307–1314.

9. Kobayashi T, Ochi M, Yanada S, Ishikawa M, Adachi N, Deie M, Arihiro K. A novel cell delivery system using magnetically labeled mesenchymal stem cells and an external magnetic device for clinical cartilage repair. *Arthroscopy*. 2008; 24(1): 69–76.

10. Kobayashi T, Ochi M, Yanada S, Ishikawa M, Adachi N, Deie M, Arihiro K. Augmentation of degenerated human cartilage in vitro using magnetically labeled mesenchymal stem cells and an external magnetic device. *Arthroscopy*. 2009; 25(12): 1435–1441.

11. Kamei G, Kobayashi T, Ohkawa S, Kongcharoensombat W, Adachi N, Takazawa K, Shibuya H, Deie M, Hattori K, Goldberg JL, et al. Articular cartilage repair with magnetic mesenchymal stem cells. *Am J Sports Med*. 2013; 41(6): 1255–1264.

12. Barbash IM, Chouraqui P, Baron J, Feinberg MS, Etzion S, Tessone A, Miller L, Guetta E, Zipori D, Kedes LH, et al. Systemic delivery of bone marrow-derived mesenchymal stem cells to the infarcted myocardium: feasibility, cell migration, and body distribution. *Circulation*. 2003; 108(7): 863–868.

13. Fischer UM, Harting MT, Jimenez F, Monzon-Posadas WO, Xue H, Savitz SI, Laine GA, Cox CS Jr. Pulmonary passage is a major obstacle for intravenous stem cell delivery: the pulmonary first-pass effect. *Stem Cells Dev*. 2009; 18(5): 683–692.

14. Bentzon JF, Stenderup K, Hansen FD, Schroder HD, Abdallah BM, Jensen TG, Kassem M. Tissue distribution and engraftment of human mesenchymal stem cells immortalized by human telomerase reverse transcriptase gene. *Biochem Biophys Res Commun*. 2005; 330(3): 633–640.

15. Schrepfer S, Deuse T, Reichenspurner H, Fischbein MP, Robbins RC, Pelletier MP. Stem cell transplantation: the lung barrier. *Transpl Proc*. 2007; 39(2): 573–576.

16. Lin P, Correa D, Kean TJ, Awadallah A, Dennis JE, Caplan AI. Serial transplantation and long-term engraftment of intra-arterially delivered clonally derived mesenchymal stem cells to injured bone marrow. *Mol Ther*. 2014; 22(1): 160–168.

17. Matsumoto T, Kawamoto A, Kuroda R, Ishikawa M, Mifune Y, Iwasaki H, Miwa M, Horii M, Hayashi S, Oyamada A, et al. Therapeutic potential of vasculogenesis and osteogenesis promoted by peripheral blood CD34-positive cells for functional bone healing. *Am J Pathol*. 2006; 169(4): 1440–1457.

18. Andrews NC. Disorders of iron metabolism. *N Engl J Med*. 1999; 341(26): 1986–1995.

19. Cucchiarini M, Madry H, Guilak F, Saris DB, Stoddart MJ, Koon Wong M, Roughley P. A vision on the future of articular cartilage repair. *Euro Cells Mater*. 2014; 27: 12–16.

20. Bedi A, Feeley BT, Williams RJ, 3rd. Management of articular cartilage defects of the knee. *J Bone Joint Surg Am*. 2010; 92(4): 994–1009.

21. Candela ME, Yasuhara R, Iwamoto M, Enomoto-Iwamoto M. Resident mesenchymal progenitors of articular cartilage. *Matrix Biol*. 2014; 39: 44–49.

22. Bekkers JE, Tsuchida AI, van Rijen MH, Vonk LA, Dhert WJ, Creemers LB, Saris DB. Single-stage cell-based cartilage regeneration using a combination of chondrons and mesenchymal stromal cells: comparison with microfracture. *Am J Sports Med*. 2013; 41(9): 2158–2166.

23. Chamberlain G, Fox J, Ashton B, Middleton J. Concise review mesenchymal stem cells their phenotype differentiation capacity immunological features and potential for homing. *Stem Cells*. 2007; 25: 2739–2749.

24. Semont A, Demarquay C, Bessout R, Durand C, Benderitter M, Mathieu N. Mesenchymal stem cell therapy stimulates endogenous host progenitor cells to improve colonic epithelial regeneration. *PLoS One*. 2013; 8(7): e70170.

25. Hyun JS, Tran MC, Wong VW, Chung MT, Lo DD, Montoro DT, Wan DC, Longaker MT. Enhancing stem cell survival in vivo for tissue repair. *Biotechnol Adv*. 2013; 31(5): 736–743.

26. Rustad KC, Wong VW, Sorkin M, Glotzbach JP, Major MR, Rajadas J, Longaker MT, Gurtner GC. Enhancement of mesenchymal stem cell angiogenic capacity and stemness by a biomimetic hydrogel scaffold. *Biomaterials*. 2012; 33(1): 80–90.

27. Oshima S, Ishikawa M, Mochizuki Y, Kobayashi T, Yasunaga Y, Ochi M. Enhancement of bone formation in an experimental bony defect using ferumoxide-labelled mesenchymal stromal cells and a magnetic targeting system. *J Bone Joint Surg Br*. 2010; 92(11): 1606–1613.

28. Nakabayashi A, Kamei N, Sunagawa T, Suzuki O, Ohkawa S, Kodama A, Kamei G, Ochi M. In Vivo Bioluminescence Imaging of Magnetically Targeted Bone Marrow-Derived Mesenchymal Stem Cells in Skeletal Muscle Injury Model. *J Orthop Res*. 2013; 31(5): 754–759.

29. Kodama A, Kamei N, Kamei G, Kongcharoensombat W, Ohkawa S, Nakabayashi A, Ochi M. In vivo bioluminescence imaging of transplanted bone marrow mesenchymal stromal cells using a magnetic delivery system in a rat fracture model. *J Bone Joint Surg Br*. 2012; 94(7): 998–1006.

30. Nishida K, Tanaka N, Nakanishi K, Kamei N, Hamasaki T, Yanada S, Mochizuki Y, Ochi M. Magnetic targeting of bone marrow stromal cells into spinal cord: through cerebrospinal fluid. *Neuroreport*. 2006; 17(12): 1269–1272.

31. Iso Y, Spees JL, Serrano C, Bakondi B, Pochampally R, Song YH, Sobel BE, Delafontaine P, Prockop DJ. Multipotent human stromal cells improve cardiac function after myocardial infarction in mice without long-term engraftment. *Biochem Biophys Res Commun*. 2007; 354(3): 700–706.

32. Burst VR, Gillis M, Putsch F, Herzog R, Fischer JH, Heid P, Müller-Ehmsen J, Schenk K, Fries JW, Baldamus CA, et al. Poor cell survival limits the beneficial impact of mesenchymal stem cell transplantation on acute kidney injury. *Nephron Exp Nephrol*. 2010; 114(3): e107–e116.

33. Assis AC, Carvalho JL, Jacoby BA, Ferreira RL, Castanheira P, Diniz SO, Cardoso VN, Goes AM, Ferreira AJ. Time-dependent migration of systemically delivered bone marrow mesenchymal stem cells to the infarcted heart. *Cell Transpl*. 2010; 19(2): 219–230.

34. Lee RH, Seo MJ, Reger RL, Spees JL, Pulin AA, Olson SD, Prockop DJ. Multipotent stromal cells from human marrow home to and promote repair of pancreatic islets and renal glomeruli in diabetic NOD/scid mice. *Proc Natl Acad Sci U S A*. 2006; 103(46): 17438–17443.